LC-PHSM-2001-025
February 2001

Study of Higgs Boson Production through WW–fusion at TESLA

Klaus Desch, Niels Meyer
Universität Hamburg, Germany

Abstract

We study the feasibility of measuring the cross section for Higgs boson production through the WW–fusion process, $e^+e^- \to \nu_e\bar{\nu}_e\,H^0$, at TESLA for centre–of–mass energies between 350 and 500 GeV. Realistic assumptions for detector resolution effects, b–quark tagging efficiency and background processes are made. Using the decay mode $H^0 \to b\bar{b}$ the cross section can be measured to an accuracy of approximately 3% for a Higgs boson mass of 120 GeV, assuming 500 fb^{-1} of data. This measurement can be used to extract the coupling g_{HWW} between Higgs and W bosons and to determine the total decay width of the Higgs boson.

1 Introduction

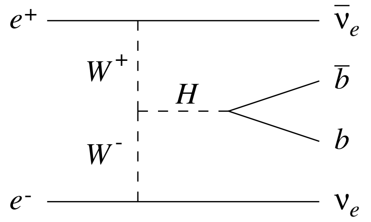

Figure 1: *WW–fusion with* $H \to b\bar{b}$ *leading to two* b*–jets and missing four momentum*

The WW–fusion process [1], $e^+e^- \to H^0\,\nu_e\bar{\nu}_e$, is one of the two major production processes for Higgs bosons at future e^+e^- colliders. Its cross section rises logarithmically with the centre–of–mass energy $\sqrt{s}$ and thus becomes dominant at large $\sqrt{s}$ while the Higgs–strahlung process, $e^+e^- \to H^0\,Z^0$ dominates at lower $\sqrt{s}$ due to its $1/s$ dependence (see Fig. 2).

The WW–fusion process directly probes the coupling g_{HWW} of the Higgs boson to W bosons. Measuring this coupling provides a possibility to determine the total decay

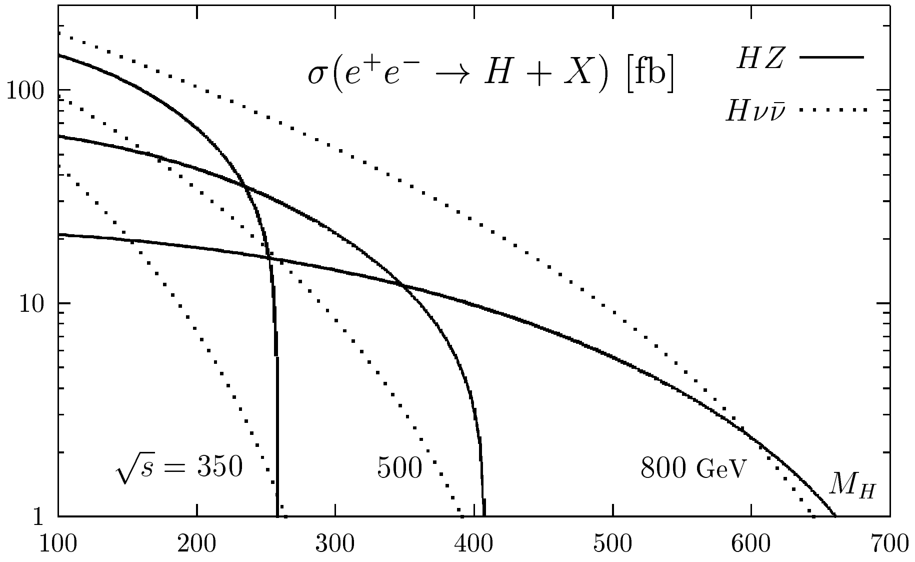

Figure 2: *Cross sections for Higgs–strahlung* $\mathrm{e^+e^-} \to \mathrm{H\,Z}$ *and WW–fusion* $\mathrm{e^+e^-} \to \mathrm{H}\,\nu\bar{\nu}$ *for various centre–of–mass energies* $\sqrt{s}$ *as functions of the Higgs boson mass* m_{H}

width of the Higgs boson with high accuracy and small model–dependence. Furthermore the measurement of g_{HWW} allows to translate the measurements of Higgs boson branching ratios into measurements of partial widths which then can be used to extract absolute values for these couplings from a global fit.

In the Standard Model ($\mathcal{SM}$), the Higgs boson decays predominantly into b–quark pairs for $m_{\mathrm{H}} \lesssim 150\,\mathrm{GeV}$. In this study we select events of the type $\mathrm{e^+e^-} \to \mathrm{b\bar{b}}\,\nu\bar{\nu}$. The selection is based on simulated events and accounts for detector effects through the TESLA parametric Monte Carlo `SIMDET` [2].

In Section 2 we describe the simulation of the signal and the relevant background processes and the selection cuts. The χ^2–fit used to extract the cross section is discussed in Section 3. The extraction of the total Higgs boson width is described in Section 4. Here, this method is also compared to alternative methods to obtain the total width. In Section 5 the impact of the g_{HWW} measurement on the overall Higgs boson profile to be determined at TESLA is shown.

2 Monte Carlo Simulation and Selection

2.1 Monte Carlo Simulation

Events from WW–fusion, Higgs–strahlung and irreducible background processes (predominantly $\mathrm{e^+e^-} \to \mathrm{Z^0Z^0} \to \nu\bar{\nu}\,\mathrm{b\bar{b}}$) were generated using `WHiZard` [3]. QCD corrections to the production cross section were accounted for by using running b–quark mass. The Higgs decay branching ratios and the total width was calculated using `HDECAY` [4]. For the hadronisation process, `PYTHIA 6.1` [5] was used.

The dominant reducible background processes (i.e. processes with final state other than

No.	Process $e^+e^- \to$	σ [fb] $\sqrt{s} = 350\,\mathrm{GeV}$	σ [fb] $\sqrt{s} = 500\,\mathrm{GeV}$
1a	$\mathrm{WW} \to \mathrm{q\bar{q}}\,\ell\nu_\ell$	5 809	3 694
1b	$\mathrm{WW} \to \mathrm{q\bar{q}}\,\mathrm{q\bar{q}}$	5 491	3 695
2	$\mathrm{W\,e}\nu \to \mathrm{q\bar{q}}\,\mathrm{e}\nu_\mathrm{e}$	2 504	4 184
3a	$\mathrm{ZZ} \to \mathrm{q\bar{q}}\,\nu\bar{\nu}$	195.4	124.9
3b	$\mathrm{ZZ} \to \mathrm{q\bar{q}}\,\ell^+\ell^-$	469.5	308.4
3c	$\mathrm{ZZ} \to \mathrm{q\bar{q}}\,\mathrm{q\bar{q}}$	190.6	126.3
4	$\mathrm{Z\,e^+e^-} \to \mathrm{q\bar{q}}\,\mathrm{e^+e^-}$	3 214	3 622
5	$\mathrm{e^+e^-} \to \mathrm{q\bar{q}}$	26 930	13 840
6	$\mathrm{e^+e^-} \to \mathrm{b\bar{b}}\,\nu\bar{\nu}$	66.1	75.5

Table 1: *Background processes considered, separated into reducible (1-5) and irreducible (6). For process 3a* b*–quarks are excluded since the corresponding process is included in process 6.*

$\mathrm{b\bar{b}}\,\nu\bar{\nu}$) were generated using `PYTHIA 6.1`. These are ZZ and WW production, single Z and single W production and two–fermion processes $\mathrm{e^+e^-} \to \mathrm{q\bar{q}}$ including $\mathrm{t\bar{t}}$. A complete list of all considered background processes is shown in Table 1.

The detector response has been simulated for all events by the fast Monte Carlo `SIMDET 3.01` [2] with parameters corresponding to the TESLA TDR.

2.2 Selection Cuts

The signal final state consists of two acoplanar jets containing B–hadron decays and large missing energy. The invariant mass of the two jets should be consistent with m_H, while no resonant behaviour of the missing mass is expected.

The following selection cuts have been applied to suppress the backgrounds:

1. Events are forced into two jets using the Durham algorithm [6]. Both jets are required to pass a b–tag criterion based on the lifetime of B–hadrons measured in the silicon vertex detector. The performance of the b–tag algorithm is described in [7] and is parametrised as a function of the jet energy and polar angle. We choose an efficiency $\epsilon_\mathrm{b} = 75\%$ for b–jets resulting in an efficient rejection of light quark jets and sufficient suppression of c–jets.

2. Only events which do not contain isolated electrons or muons of momentum larger than 5 GeV are accepted. Particles are defined to be isolated if no other charged track is reconstructed within a cone of 25° half opening angle. This cut rejects semileptonic $\mathrm{WW/ZZ} \to \mathrm{q\bar{q}}\,\ell\nu_\ell/\ell^+\ell^-$ decays.

3. The number of charged tracks should exceed 12 to reject leptonic final states and two–photon processes.

4. The total reconstructed four–momentum is required to have energy $E_{vis} < 200\,(250)\,\mathrm{GeV}$, transverse component $p_T > 10\,(5)\,\mathrm{GeV}$ at $\sqrt{s} = 350\,(500)\,\mathrm{GeV}$ and polar angle

$|\cos\theta| < 0.9$. These cuts accept events with large missing momentum and reject fully hadronic events (ZZ/WW $\rightarrow$ 4q).

5. The acoplanarity a, defined as the angle between the two reconstructed jets in the plane perpendicular to the beam axis is required to be larger than $5°$. The Durham parameter y_{23} has to be smaller than 0.01. This cut suppresses multi–jet events e.g. from fully hadronic WW, ZZ and $\mathrm{t\bar{t}}$ production.

6. The invariant mass m_{vis} of the visible event has to be consistent with the Higgs boson mass: $m_{\mathrm{H}} - 20\,\mathrm{GeV} < m_{vis} < m_{\mathrm{H}} + 10\,\mathrm{GeV}$. The effect of this cut on the signal and the background processes is shown in Fig. 3.

7. Since the cross section of most of the reducible background processes is higher at $\sqrt{s} = 350\,\mathrm{GeV}$ for this centre–of–mass energy additional cuts are applied: the visible reconstructed energy E_{vis} is required to be larger than 100 GeV, the angle α between the two jets should satisfy $\cos\alpha < 0.2$ and the Durham parameter y_{34} is required to satisfy $y_{34} < 0.01$.

	W eν	WW	Z ee	ZZ	$\mathrm{q\bar{q}}$
no cuts $\times 10^3$	1252/2093	5651/3696	1607/1811	4278/2798	13400/6900
b–tag	1050/1450	66300/39630	29940/14150	23490/11570	466090/694410
isol. e, μ	1050/1450	59860/33190	11490/5570	18620/9170	455680/665830
# tracks	990/1290	12700/8110	9820 /4750	2790 /1710	222190/390410
E_{vis}	900/1160	380/8110	6260/4710	200/1710	70970/368950
p_T	870/1120	330/4730	2420/2500	190/1270	15640/161950
$\|\cos\theta\|$	870/1120	330/3990	2420/2500	190/1270	15640/39980
a ,($\cos\alpha$)	390/1090	190/2360	410/1010	60/480	830/5350
y_{23} ,(y_{34})	330/1000	90/820	220/490	30/230	120/1440
$m_{vis}\,(m_{\mathrm{H}} = 120)$	30/30	30/70	70/140	10/0	20/80
$m_{vis}\,(m_{\mathrm{H}} = 160)$	0/0	10/20	10/40	10/10	30/60

Table 2: *Cut flow table showing the effect of the cuts on the reducible background processes. Numbers of events are given for* $\int\mathcal{L} = 500\,\mathrm{fb}^{-1}$ *and* $\sqrt{s} = 350/500\,\mathrm{GeV}$. *Note that the numbers in the first row are scaled by a factor of* 10^{-3}.

The selection has been optimised using a sample of all reducible background processes corresponding to $\int\mathcal{L} = 50\,\mathrm{fb}^{-1}$. The event numbers were scaled up to correspond to $500\,\mathrm{fb}^{-1}$. The effect of the cuts is shown in Table 2. It can be seen that all reducible backgrounds can be suppressed by several orders of magnitude. Their contribution to the total background only adds up to $\mathcal{O}(100)$ events for $500\,\mathrm{fb}^{-1}$. Note, that the $\mathrm{q\bar{q}}$ numbers include the $\mathrm{t\bar{t}}$ background.

2.3 Irreducible Background Processes

The reaction $\mathrm{e^+e^-} \rightarrow \mathrm{b\bar{b}}\,\nu\bar{\nu}$ receives contributions from more than 20 tree level diagrams including Higgs–strahlung $\mathrm{e^+e^-} \rightarrow \mathrm{HZ} \rightarrow \mathrm{b\bar{b}}\,\nu\bar{\nu}$ and WW–fusion. In the case of $\nu = \nu_{\mathrm{e}}$ interference between Higgs–strahlung and the WW–fusion signal occurs, which is predicted to decrease the total Higgs boson production cross section [8] at the centre–of–mass energies and Higgs boson masses under consideration. In order to extract the g_{HWW} coupling, the interference term has to be considered. After applying the selection cuts, its contribution is only $\mathcal{O}(0.1\%)$ of the signal cross section and therefore it has been neglected in this study. The inclusion of the interference complicates the analysis slightly but it can be treated correctly without any principal problem.

	$\mathrm{e^+e^-} \to \mathrm{H}\,\nu\bar{\nu}$	$\mathrm{e^+e^-} \to \mathrm{HZ}$	$\mathrm{e^+e^-} \to \mathrm{bb}\,\nu\bar{\nu}$
no cuts	11340/27030	9000/3960	33040/37740
b–tag	6289/15202	5098/2232	15339/21254
isol. e, μ	6289/15202	5098/2232	15335/21248
# tracks	5986/14478	4865/2128	14177/19547
E_{vis}	5745/14098	4807/2073	12396/17413
p_T	5591/13999	4780/2057	12034/16616
$\lvert\cos\theta\rvert$	4448/10420	3935/1537	9716/9734
a ,$(\cos\alpha)$	3925/9913	3785/1464	4890/9445
y_{23} ,(y_{34})	3916/9887	3774/1460	4879/9422
m_{vis}	3379/8361	3184/1236	346/386

Table 3: *Cut flow table for all processes contributing to the* $\mathrm{b\bar{b}}\,\nu\bar{\nu}$*–final state: WW–fusion* $\mathrm{e^+e^-} \to \mathrm{H}\,\nu\bar{\nu} \to \mathrm{b\bar{b}}\,\nu\bar{\nu}$, *Higgs–strahlung* $\mathrm{e^+e^-} \to \mathrm{HZ} \to \mathrm{b\bar{b}}\,\nu\bar{\nu}$ *and other irreducible background processes* $\mathrm{e^+e^-} \to \mathrm{b\bar{b}}\,\nu\bar{\nu}$. *Numbers are given for* $\mathcal{L} = 500\,\mathrm{fb}^{-1}$, $m_{\mathrm{H}} = 120\,\mathrm{GeV}$ *and* $\sqrt{s} = 350/500\,\mathrm{GeV}$.

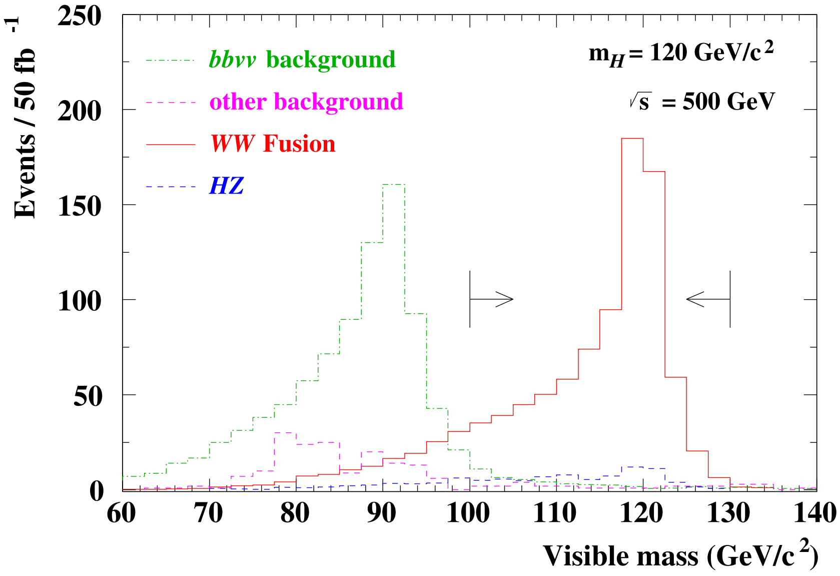

Figure 3: *Distributions of the invariant mass* m_{vis} *of the reconstructed events after the selection. Tails to lower masses in WW–fusion,* HZ *and* $\mathrm{b\bar{b}}\,\nu\bar{\nu}$ *background are due to neutrinos in leptonic* b– *and* c*–quark decays.*

All processes $\mathrm{e^+e^-} \to \mathrm{b\bar{b}}\,\nu\bar{\nu}$ without Higgs bosons (irreducible background) have a total cross section which is three orders of magnitude smaller than the total reducible background. However, the suppression by the cuts is less effective. The effect of the selection cuts on the WW–fusion signal, Higgs–strahlung and other irreducible backgrounds is shown in Table 3. The selection efficiency for WW–fusion events with $m_{\rm H} = 120\,\rm GeV$ is approximately 30%. The number of selected Higgs–strahlung events is approximately the same as the signal at $\sqrt{s} = 350\,\rm GeV$ and only 15% of the signal at $\sqrt{s} = 500\,\rm GeV$. The other $\rm b\bar{b}\,\nu\bar{\nu}$ backgrounds amount to approximately 10% (5%) of the signal at 350 (500) GeV.

3 Fit and Cross Section Results

The contributions of signal and background[1] ($\rm e^+e^- \to b\bar{b}\,\nu\bar{\nu}$ and $\rm e^+e^- \to HZ \to b\bar{b}\,\nu\bar{\nu}$) to the events passing the selection are determined from a χ^2 fit to the distribution of the missing mass, m_{mis}. This distribution is expected to exhibit a peak at $m_{mis} = m_{\rm Z}$ both for HZ and ZZ events while a wide–spread spectrum peaking at large m_{mis} is expected for signal events (see Fig. 4).

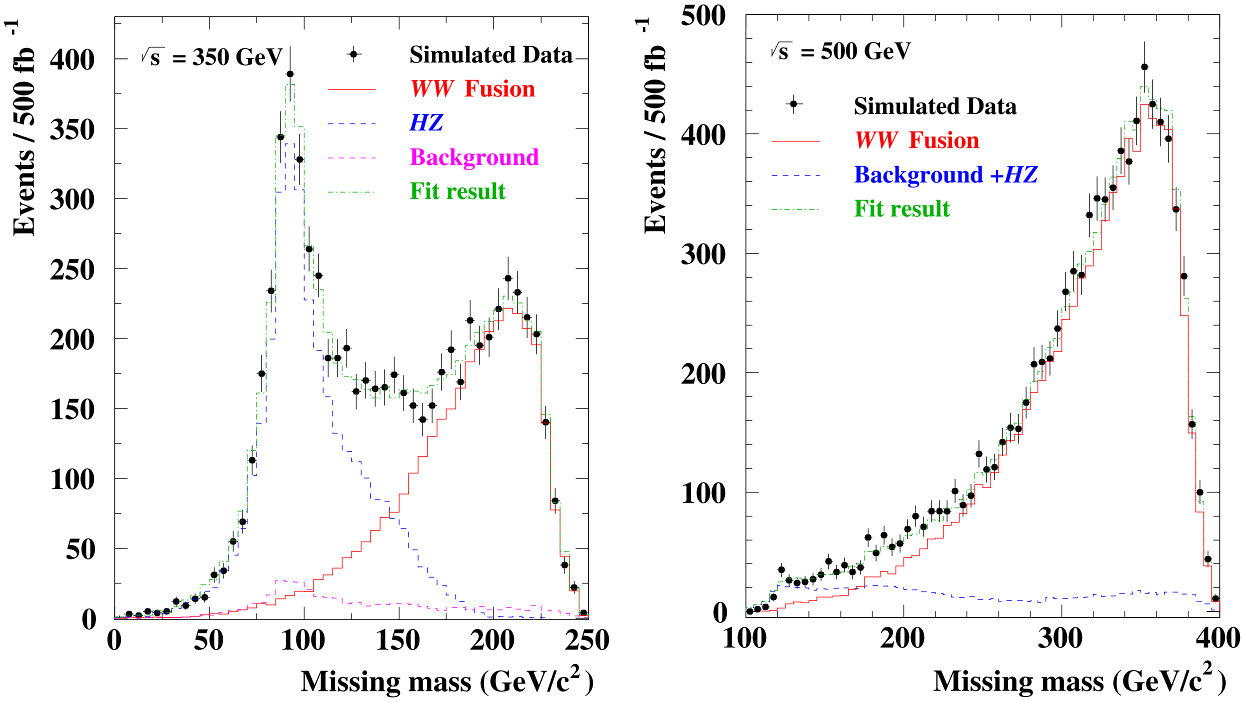

Figure 4: *Results of a fit to the missing mass distribution for events passing all selection cuts for $m_{\rm H} = 120\,\rm GeV$ at $\sqrt{s} = 350/500\,\rm GeV$. For $\sqrt{s} = 500\,\rm GeV$, the dashed curve for background contains both non–Higgs $\rm b\bar{b}\,\nu\bar{\nu}$–background and Higgs–strahlung, the latter being dominant.*

The result of the fit yields the cross section $\sigma_{\rm WW-fusion}(\rm H \to b\bar{b})$ for WW–fusion times the branching ratio $\rm BR(H \to b\bar{b})$ of Higgs bosons to b–quarks since only $\rm H \to b\bar{b}$ decays are selected. The total WW–fusion cross section is obtained by division through the branching ratio $\rm BR(H \to b\bar{b})$. This measurement can be carried out at TESLA

[1] The small contributions from the interference and from the reducible background have been neglected.

$\sqrt{s}$	m_{H}	Δfit	$\Delta\mathrm{BR}(\mathrm{H}\to\mathrm{b\bar{b}})^{\dagger}$	$\Delta\sigma_{\mathrm{WW-fusion}}$
350	120	2.2%	2.5%	3.3%
	140	4.0%	3.1%	4.7%
	160	– *	– *	– *
500	120	1.3%	2.5%	2.8%
	140	2.0%	3.1%	3.7%
	160	7.0%	10.6%	13.0%

Table 4: *Result of the fit and accuracy on the total cross section for WW–fusion.* †*: Numbers taken from [9, 10]* **: Too few events for reasonable fit*

independently, using Higgs–strahlung events only [9, 10]. Combining with the expected uncertainty on $\mathrm{BR}(\mathrm{H}\to\mathrm{b\bar{b}})$ accuracies of 2.8% to 13% can obtained for $120\,\mathrm{GeV} \le m_{\mathrm{H}} \le 160\,\mathrm{GeV}$ (see Table 4).

3.1 Beam Polarisation

By choosing a completely left–handed polarised electron beam the signal cross section is enhanced by a factor two due to the purely left–handed coupling of the W^- to the electron. Another factor of two can be obtained by choosing a completely right–handed polarised positron beam in addition. We have investigated the accuracy achievable for the WW–fusion cross section for two realistic beam polarisation scenarios: a) $P_{\mathrm{e}^-} = 80\%$, $P_{\mathrm{e}^+} = 0$ and b) $P_{\mathrm{e}^-} = 80\%$, $P_{\mathrm{e}^+} = 45\%$ at $\sqrt{s} = 500\,\mathrm{GeV}$. The polarised events have been generated using the beam polarisation feature of the `WHIZARD` generator, therefore also angular distributions are treated correctly.

m_{H}	$P_{\mathrm{e}^-} = 80\%$ $P_{\mathrm{e}^+} = 0$	$P_{\mathrm{e}^-} = 80\%$ $P_{\mathrm{e}^+} = 45\%$
120	0.9%	0.8%
140	1.4%	1.2%
160	5.1%	4.2%

Table 5: *Results for the measurement error $\Delta\sigma$ of $\sigma_{\mathrm{WW-fusion}}$ in the case of polarised electron and/or positron beams for $500\,\mathrm{fb}^{-1}$ at $\sqrt{s} = 500\,\mathrm{GeV}$.*

The results are in good agreement with the hypothesis, that the relative error scales like $1/\sqrt{N}$ as a function of the number N of observed events only. It is however unlikely, that the full luminosity of TESLA will be spent in the polarisation mode which is optimal for this measurement. Still, polarisation is beneficial for this analysis, since the cross section of the signal and the dominant backgrounds scale differently with the choice of beam polarisation. This behaviour can be used to disentangle them with only limited use of Monte Carlo thus reducing the systematic uncertainties.

4 Extraction of the Total Higgs Boson Width

Both the cross section for WW–fusion $\sigma_{\mathrm{WW-fusion}}$ and the partial width $\Gamma(\mathrm{H}\to\mathrm{WW})$ can be expressed in terms of the coupling g_{HWW} of the Higgs boson to W bosons [11]. In the high energy approximation $\sqrt{s} \gg 2\,m_{\mathrm{W}}$ the cross section is given by

$$\sigma_{\mathrm{WW-fusion}} \longrightarrow \frac{g^2_{\mathrm{HWW}}\, G_F^2}{32\,\pi^3} \left[\left(1 + \frac{m^2_{\mathrm{H}}}{s}\right) \log \frac{s}{m^2_{\mathrm{H}}} - 2\left(1 - \frac{m^2_{\mathrm{H}}}{s}\right) \right]$$

and the partial width is given by

$$\Gamma(\mathrm{H} \to \mathrm{WW}) = \frac{g^2_{\mathrm{HWW}}\, m^3_{\mathrm{H}}}{64\,\pi\, m^2_{\mathrm{W}}} \left(1 - \frac{4\,m^2_{\mathrm{W}}}{m^2_{\mathrm{H}}} + \frac{12\,m^4_{\mathrm{W}}}{m^4_{\mathrm{H}}}\right) \left(1 - \frac{4\,m^2_{\mathrm{W}}}{m^2_{\mathrm{H}}}\right)^{1/2}.$$

Therefore, the measurement of $\sigma_{\mathrm{WW-fusion}}$ can be translated into a measurement of $\Gamma(\mathrm{H} \to \mathrm{WW})$. This translation is almost free of model assumptions. The total decay width Γ_{tot} can be obtained using the relation $\Gamma(\mathrm{H} \to \mathrm{WW}) = \Gamma_{tot} \times \mathrm{BR}(\mathrm{H} \to \mathrm{WW})$. Again, the branching ratio $\mathrm{BR}(\mathrm{H} \to \mathrm{WW})$ can be measured independently, from Higgs–strahlung events [10, 12].

In a similar way, the indirect determination of the total Higgs decay width is possible by measuring the di–photon partial width through the process $\gamma\gamma \to \mathrm{H}$ at the $\gamma\gamma$ collider [13, 14] and the decay branching ratio $\mathrm{BR}(\mathrm{H} \to \gamma\gamma)$ [15].

Finally a third, although less model independent method exists for the determination of Γ_{tot}: the partial WW–width $\Gamma(\mathrm{H} \to \mathrm{WW})$ can be calculated from the precisely measurable Higgs-strahlung cross section (which is only a function of g_{HWW}) using the SU(2) relation $g_{\mathrm{HWW}} = g_{\mathrm{HZZ}} \cos^2\theta_W$. This measurement is then again combined with the $\mathrm{BR}(\mathrm{H} \to \mathrm{WW})$ measurement.

m_{H}	$\Delta\Gamma_{tot}$ using g_{HWW}	$\Delta\Gamma_{tot}$ using $g_{\mathrm{H}\gamma\gamma}$	$\Delta\Gamma_{tot}$ using $g_{\mathrm{HZZ}} \propto g_{\mathrm{HWW}}$
120	6.1%	14.1%	5.9%
140	4.5%	— *	4.1%
160	13.4%	— *	3.9%

Table 6: *Comparison of the different methods for determining the total Higgs width $\Gamma_H(tot)$. *: No numbers available*

The results of the three methods are shown in Table 6. It can be seen that the model independent method using g_{HWW} and the method using $g_{\mathrm{HWW}} \propto g_{\mathrm{HZZ}}$ are similar in accuracy while the method using $g_{\mathrm{H}\gamma\gamma}$ is limited by the precision achievable on $\mathrm{BR}(\mathrm{H} \to \gamma\gamma)$.

5 The g_{HWW} Coupling and Implications

The precise knowledge of the g_{HWW} coupling plays an important role in the determination of the complete Higgs profile. In particular the couplings to fermions ($\mathrm{b\bar{b}}$, $\mathrm{c\bar{c}}$, $\tau^+\tau^-$) are probed in the measurement of the corresponding branching ratios. The absolute value of the coupling can however only be determined if the total decay width is known (see Section 4).

Alternatively, using the available information in the most efficient way, a global fit can be performed to extract the couplings from all measurements of branching ratios and production cross sections simultaneously [16]. In this approach, the importance of the WW–fusion cross section measurement can be clearly seen from in Fig. 5. The huge correlation e.g. between $g_{\mathrm{Hb\bar{b}}}$ and g_{HWW} which is present if only the branching ratios and the Higgs–strahlung cross section are available is drastically reduced when the WW–fusion measurement is added.

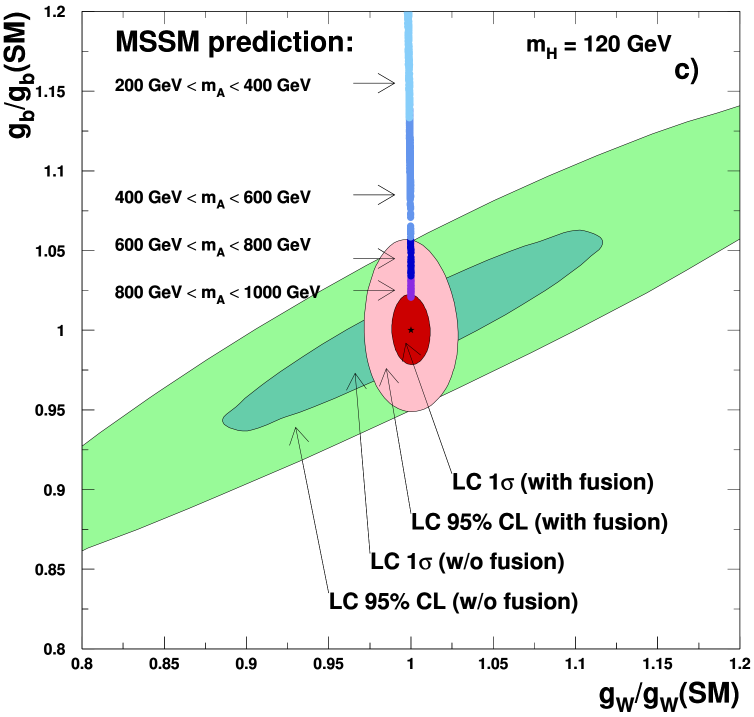

Figure 5: *A global fit of the $g_{\mathrm{Hb\bar{b}}}$ and g_{HWW} couplings. The couplings are shown relative to their $\mathcal{SM}$ predictions. Shown are the 1σ and 95% C.L. error contours when only the branching ratio measurements (into $\mathrm{b\bar{b}}$, $\mathrm{c\bar{c}}$, $\tau^+\tau^-$ and $\gamma\gamma$) and the cross sections for* ZH *and* $\mathrm{t\bar{t}H}$ *production are used (large contours) and when the WW–fusion cross section measurement is added (small contours). For further details see [16].*

6 Summary And Conclusions

We present a simulation of the measurement of the cross section for the WW–fusion processes for light Higgs bosons, $m_{\mathrm{H}} = 120 - 160\,\mathrm{GeV}$. This cross section can be measured at TESLA with a precision of approximately 3% (13%) for $m_{\mathrm{H}} = 120\,(160)\,\mathrm{GeV}$ using $500\,\mathrm{fb}^{-1}$at $\sqrt{s} = 500\,\mathrm{GeV}$. For Higgs boson masses below 150 GeV, the measurement can also be performed at $\sqrt{s} = 350\,\mathrm{GeV}$ with slightly larger errors.

Since this study only uses $\mathrm{H} \to \mathrm{b\bar{b}}$ decays it is only applicable to Higgs boson masses below 160 GeV. This limitation could be overcome by selecting $\mathrm{H} \to \mathrm{WW}$ decays.

This measurement provides the best almost model–independent way to determine the total decay width of the Higgs boson (with accuracy $\mathcal{O}(5\%)$) in the mass range under consideration. This allows to determine the absolute values of Higgs boson couplings to fermions from their corresponding branching ratios at the percent level.

References

[1] D.R.T. Jones and S. Petcov. *Phys. Lett.* **B84** (1979), 440;
R. Cahn and S. Dawson. *Phys. Lett.* **B136** (1984), 196;
G. Kane, W. Repko, and W. Rolnick. *Phys. Lett.* **B148** (1984), 367;
G. Altarelli, B. Mele, and F. Pitolli. *Nucl. Phys.* **B287** (1987), 205;
W. Kilian, M. Krämer, and P.M. Zerwas. *Phys. Lett.* **B373** (1996), 135.

[2] M. Pohl and H.J. Schreiber. *SIMDET – A Parametric Monte Carlo for a TESLA Detector*, DESY 99–030.

[3] W. Kilian. *WHiZard Manual*, LC–TOOL–2001–039.

[4] A. Djouadi, M. Spira, and P.M. Zerwas. *Z. Phys.* **C70** (1996), 427;
A. Djouadi, J. Kalinowski, and M. Spira. *Comp. Phys. Comm.* **108** (1998), 56.

[5] T. Sjöstrand et al. *High–Energy–Physics Event Generation with PYTHIA 6.1*, LU–TP 00–30 and hep–ph/0010017.

[6] Y. Dokshitzer. *J. Phys.* **G17** (1991), 1537;
N. Brown and W.J. Stirling. *Phys. Lett.* **B252** (1990), 657;
S. Bethke et al. *Nucl. Phys.* **B370** (1992), 310;
S. Catani et al. *Phys. Lett.* **B269** (1991), 432;
N. Brown and W.J. Stirling. *Z. Phys.* **C53** (1992), 629.

[7] R. Hawkings, *Vertex Detector and Flavour Tagging Studies for the TESLA Linear Collider*, LC–PHSM–2000–021.

[8] W. Kilian, M. Krämer, and P. M. Zerwas. *Phys. Lett.* **B373** (1996), 135.

[9] M. Battaglia. In “Proc. of the Worldwide Study on Physics and Experiments with Future e^+e^- Linear Colliders”, E. Fernandez and A. Pacheco (editors), UAB, Barcelona 2000, Vol. I, 163 and M. Battaglia, to appear in e^-Eur. Phys. J..

[10] E. Boos, V. Ilyin, A. Pukhov, M. Sachwitz, and H.J. Schreiber. *Eur. Phys. J.* **C5** (2000), 1;
E. Boos, V. Ilyin, A. Pukhov, M. Sachwitz, and H.J. Schreiber. *Branching Fraction Measurements of the $\mathcal{SM}$ Higgs with a Mass of 160* GeV *at Future Linear* e^+e^- *Colliders*, LC–PHSM–2000–035.

[11] see e.g. M. Spira and P.M. Zerwas. *Electroweak Symmetry Breaking and Higgs Physics*, hep–ph/9803257v2.

[12] G. Borisov and F. Richard. *Precise Measurement of Higgs Decay Rate into* WW* *at Future* e^+e^- *Linear Colliders and Theoretical Consequences*, LAL 99–26 and hep–ph/9905413.

[13] G. Jikia and S. Söldner–Rembold. *Nucl. Phys* (Proc. Suppl.) **82** (2000), 373;
G. Jikia and S. Söldner–Rembold. *Light Higgs Production at a Photon Collider*, LC–PHSM–2001–060.

[14] M. Melles, W.J. Stirling, and V.A. Khoze. *Phys. Rev.* **D61** (2000), 54015.

[15] E. Boos, J.C. Brient, D.W. Reid, H.J. Schreiber, and R. Shanidze. *Measuring the Higgs Branching Fractions into two Photons at Future Linear* e^+e^- *Colliders*, DESY–00–162 and LC–PHSM–2000–053.

[16] K. Desch and M. Battaglia. *Determination of the Higgs Profile: HFITTER*, LC–PHSM–2001–053.